論文

# 나노인덴테이션 해석을 통한 Ag/Cu층에서 발생하는 Misfit 전위의 slip 특성에 대한 연구

트란딘 롱*, 유용문**, 전성식*+

# Nanoindentation on the Layered Ag/Cu for Investigating Slip of Misfit Dislocation

Long Trandinh*, Yong-Moon Ryu** and Seong Sik Cheon*+

## ABSTRACT

The EAM simulation of nanoindentation was performed to investigate misfit dislocation slip in the Ag/Cu. The film layer, whose thickness in the range of 2-5nm, was indented by a spherical indenter with the Nóse-Hoover thermostat condition. The simulation shows that the indentation position relative to misfit dislocation (MFD) has the effect on the dislocation, glide up or cross slip, for Ag film layer thickness less than 4 nm. Elastic energy variation during MFDs slip was revealed to be a key factor for the softening of Ag/Cu. The critical film layer thickness was evaluated for each case of Ag/Cu according to the spline extrapolation technique.

## 초 록

Ag/Cu층에서 발생하는 misfit 전위를 분석하기 위하여, EAM기법을 활용한 나노인덴테이션 해석을 수행하였다. Nóse-Hoover 서모스텟 조건에 의거하여, 2-5nm 정도의 두께를 갖는 필름층에 구형 인덴터로 압입하였다. 해석결과는 misfit 전위에 대한 상대적인 압입위치가, 4nm이하의 필름에 대하여 영향을 미치는 것으로 나타났다. 전위에 의한 슬립 발생할 때 탄성에너지 변화는 Ag/Cu의 연화의 중요한 변수로 작용하며, 각각의 경우에 대하여 임계필름두께에 대해서도 고찰하였다.

**Key Words :** 원자해석(Atomistic simulation), 나노인덴테이션(Nanoindentation), 미스핏 전위(Misfit dislocation), 전위 크로스 슬립(Dislocation cross slip)

## 1. Introduction

Nano-silver with significant characteristics such as light reflection, electric conductivity and antibacterial has been used for medical, optical equipments and electronic appliances [1-6]. Nanometer Ag film/Cu that inherits significant characteristics of nano-silver in hope will promise to be more widely applied. Therefore, the knowledge about mechanical properties of Ag/Cu is very necessary for beyond applications. Similar to layered structures, the mechanical properties of Ag/Cu are handled by the interface as well as misfit dislocation (MFD) due to lattice mismatch [7]. Mechanical properties are affected by film layer thickness as grain size in poly-crystal materials [8,9], the yield strength of multilayered materials is found to be proportional to the inverse square root of grain size as the Hall-Petch relation [10,11]. Under certain applied

접수: 2011년 2월 20일, 게재승인: 2011년 5월 9일
* Division of Mechanical and Automotive Engineering, Kongju National University
** Korea Automotive Technology Institute
*+ Corresponding author(E-mail:sscheon@kongju.ac.kr)

loads, dislocations are nucleated in a grain, move toward and interact with grain boundary. The interaction force between them that is often repulsive [12], will prevent dislocations motion and resulted in piling up at the grain boundary. The more dislocations pile up at interface the more obstacles are nucleated to block dislocation motion, which is a condition for plastic deformation. Nevertheless, if grain size is less than the value, the critical grain size, dislocations can transmit through the boundary due to repulsive force between dislocations greater than the damping of the boundary and resulted in the softening of poly-crystal materials as well as multilayered materials [13-17]. Therefore, the critical grain size is a key factor for understanding characteristics of multilayered materials. The study on Ni (001)/Cu(001), which is similar to the structure in this work, was performed Saraev and Miller [18]. The nanoindentation simulation [19,20] using embedded atom method (EAM) [21-23] shows that the placement of the indenter relative to the MFD array determines dislocation pile-ups or transmission through the interface. It also reveals the effect of surface layer thickness on the interactions between MFD and dislocation nucleated from indentation. Besides, environment condition such as temperature is considered to be a factor affects Ag/Cu properties such as the interface scattering factor or conductivity depending on temperature [24-26]. However, MFD slip in Ag/Cu and their effect on mechanical properties are not fully understood.

In the present study, atomistic simulations of nanoindentation on Ag (001)/Cu (001) were performed to investigate MFD slip. The film layer thickness in the range from 2 to 5 nm with a constant substrate layer thickness was chosen for indentation by the 4 nm spherical indenter tip at two positions relative to the MFD. The simulation shows the onset of yielding indentation force increases with increment of film layer thickness as the softening phenomenon. The dislocation is affected by the indentation position for very thin film layer associated with relation between film layer thickness and indenter size. Slip of MFD was revealed a key factor for the softening phenomenon through analysis of the elastic energy variation, and critical film layer thickness was calculated from the results of film/substrate and bulk material.

## 2. Simulation detail

The constant substrate layer thickness of 7 nm, both lateral lengths of 12 nm and film layer thickness from 2 to 5 nm were chosen for modeling the Ag film/Cu substrate material. For the sake of brevity, the name of models is shortened by closing the film layer thickness without unit following name of film. For instance, Ag5/Cu is 5 nm Ag film/Cu substrate. As a result, the models were named Ag2/Cu, Ag3/Cu, Ag4/Cu and Ag5/Cu. The crystalline direction (001) was employed for the both layers. The initial slit between these two layers was set to be 0.1925 nm, equivalent to the average of halves of lattice constants, which are equal to 0.409 and 0.361 nm for Ag and Cu, respectively [27]. The selection value for the slit will not affect the simulation result since it is rearranged in an equilibrium process by interatomic forces between atoms. In this work, the embedded atom method (EAM) potential [28] was employed for describing the interaction between the same type of atoms Cu-Cu and Ag-Ag, and the Johnson's formula [29] for different type of atoms, Cu-Ag, as follows:

$$\phi_{AB}(r)=\frac{1}{2}\left(\frac{f_B(r)}{f_A(r)}\phi_{AA}(r)+\frac{f_A(r)}{f_B(r)}\phi_{BB}(r)\right) \tag{1}$$

where $\phi_{AB}$ is the pair potential energy between an atom type A and an atom type B and *f(r)* is the electric density function. The interaction between an atom and the rigid 4 nm spherical indenter was described by the atomistic force as below [30]:

$$F(r)=-k(r-r_0)^2 \tag{2}$$

where $k$ is the force constant, $r$ is the distance between an atom and the indenter centre and $r_0$ is the radius of the indenter. The force was applied for all atoms contact with the indenter, and equal to zero for noncontact atoms. The force constant was explicit for calculating indentation force and chosen based on stiffness of the indenter tip. Therefore, the value of 10 eV/Å$^3$, the same as suggestion of Lilleodden et al [31], was chosen for the force constant in this study. Indentation was simulated at the temperature T = 10 K by displacing the indenter into the model in 0.1 Å steps, minimizing the system energy, and then evaluating the indentation force. Prior to indentation, the model must be spent the equilibrium process using a Nóse-Hoover thermostat [32,33] for 40 ps with the time step of $10^{-3}$ ps. The nanoindentation simulations were carried out by the parallel molecular dynamics

program LAMMPS [34] with the periodic boundary condition for side surfaces and the fixed for the bottom. In order to compare indentation behaviors of film/substrate with those of the bulk materials of film and substrate, bulk Ag and Cu models with dimensions 12×12×10 nm were also performed.

An attention in simulation layered material is the selecting lateral length for models since existence of mismatch between these layers. That length needs to certify two conditions, one is the smallest initial strain, it means that the difference of the lateral lengths between layers is smallest or equal zero in a perfect case. The other is to be met the boundary condition, in other word, the lateral length of a layer must be equal to multiple of the lattice constant of the layer material. Therefore, the length for the case of both layers with the same crystal direction of (001) can be chosen from the following equation:

$$l = n_s a_s = n_f a_f \tag{3}$$

where $n$ is multiple of the lattice constant, a, of substrate layer, $s$, and the film layer, $f$. In this work, the both lateral lengths approximately 12 nm as mentioned above with initial strain about 0.03% were chosen the same as the previous study [35]. The lattice mismatch will create local deformation in the interface of two layers in form of misfit dislocations (MFDs). The MFDs of two FCC metal layers, Ag, Cu, with the same crystal direction (001) are formed along the slip directions [110] in the interface to create the MFD network as shown in Fig. 1 [35]. The indenter position relative to MFD may affect simulation results since interaction between dislocations, attractive, repulsive or neutral, is quit sensitive with dislocations position. Therefore, the indentation was carried out at the position exactly above the intersection node of two MFDs, nodded indentation, and the space surrounded by MFDs for spaced indentation as illustrated in Fig. 1.

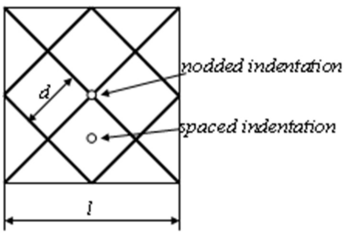


**Fig. 1 MFD network in the interface of FCC metal (001)/FCC metal (001) materials and indenter position relative to MFD, misfit spacing, d, is distance between two closest parallel MFDs.**

## 3. Results and Discussion

### 3.1 Indentation force

Indentation force was achieved by summing atomic forces of atoms contacted to the indenter at every steps displaced the constant depth in the model. The indentation was evaluated to stop at the depth of 10 Å since the models already initiated plastic deformation. Moreover, indentation force is not dependent on the indentation position relative to MFD [18]. The force-depth curves of Ag/Cu, bulk Ag and bulk Cu under nodded indentation were only shown in Fig.2, in which the Cu curve, represented for bulk Cu, is clearly higher than the Ag curve for bulk Ag. The force drop occurred at the depth of 8.7 Å, 7.8 Å in the Ag, Cu curves, respectively, by initiating plastic deformation [30, 36]. The drop happened earlier for Ag/Cu by MFD action which is the cause of the softening in layered material, and the depth at drops in the curves and the yield force at the peak before drop were listed in Table 1. It shows the yield force increases with increasing film layer thickness.

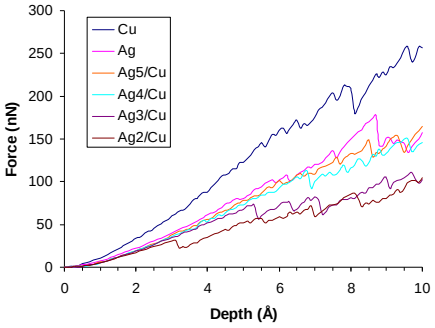


**Fig. 2 Force-depth curves of Ag/Cu, bulk Ag and Cu.**

**Table 1 indentation depth and yield force at drop**

| Model | Depth(Å) | Yield force(nN) |
|---|---|---|
| Ag2/Cu | 3.1 | 31.63 |
| Ag3/Cu | 5.1 | 72.64 |
| Ag4/Cu | 6.6 | 112.42 |
| Ag5/Cu | 8.5 | 149.33 |
| Ag | 8.7 | 177.83 |
| Cu | 7.8 | 212.25 |

### 3.2 Defect structure

#### 3.2.1 Defect identification

Defect structures were attracted from simulation at very indentation step by centrosymmetry parameter method [30].

At an indentation step, all atoms were calculated their centrosymmetry parameter by the following equation:

$$P = \sum_{i=1}^{6} \left| \boldsymbol{R}_i + \boldsymbol{R}_{i+6} \right|^2 \quad (4)$$

where $R_i$ and $R_{i+6}$ are the six pairs of opposite nearest neighbor vectors. The defect structures were presented by plotting only atoms in defects. The red atoms with P in the range 0.5 Å$^2$-5 Å$^2$ represents for dislocation, the yellow ones with P in the range 5 Å$^2$-18 Å$^2$ for stacking fault and free surfaces by black dots with P greater than 18 Å$^2$.

### 3.2.2 Bulk materials

Study defect structures during indentation shows defect evolution in bulk Cu is the same as that of bulk Ag. Thus, defect structures in bulk Ag shown in Fig. 3 can present for those in bulk Cu. The first, the dislocation was homogeneously nucleated in the form of the pyramidal defect structure which is constructed by four triangular stacking faults on slip planes (111) and four stair-rod dislocations (Lomer-Cottrell dislocations) at the sides and four Shockley partial dislocations along <110> directions on the top as shown in Fig. 3 (a) and (b). The second, two tetrahedral defect structures were nucleated on two opposite faces of the pyramidal defect structure, and the defect zone gradually transformed into the dihedral defect structure [37]. Analysis of this structure in Fig. 3 (d) shows it is a sessile lock with the stair-rod dislocation at about 2.38 nm depth from the top surface. Then, defect developed at the stair-rod dislocation and glided in a slip plane of the sessile lock toward the bottom to form the embryonic dislocation loops as shown in Fig. 3 (e).

The glide down of the embryonic dislocation loop, Shockley partial dislocations, nucleated plastic deformation and represented on force-depth curve by a drop at the depth of 8.7 Å, 7.8 Å in the Ag, Cu curves, respectively, as mentioned above. Analysis of defect evolution shows actions of dislocation conforms to Frank's law for FCC metal such as dislocations were nucleated along slip directions <110> and glided in slip planes (111). Therefore, we can consume that defect evolution in bulk Ag and Cu is only handled by crystal structure.

### 3.2.3 Ag/Cu materials

Evolution from the pyramidal defect structure to the embryonic defect loops were only influenced by crystal structure as mentioned above. Therefore, investigation defect evolution in Ag/Cu material

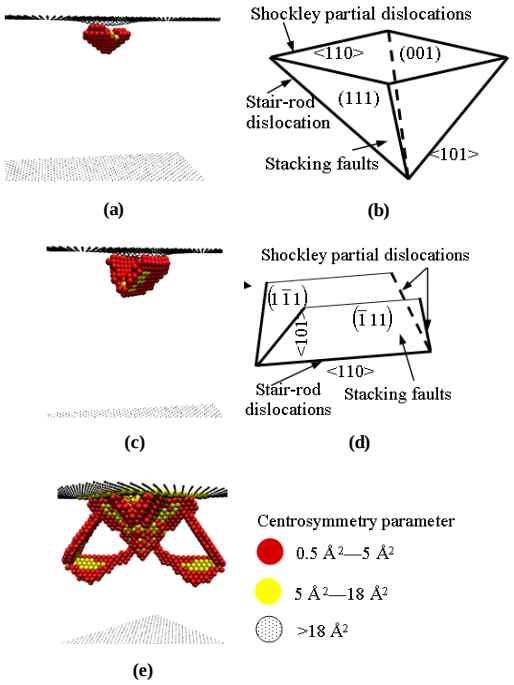


**Fig. 3 Defect evolution in bulk Ag (a) pyramidal defect structure, (b) dislocation analysis of the pyramid (c) dihedral defect structure, (d) sessile lock illustration of the dihedral, and (e) the embryonic dislocation loops.**

focused on motions of MFDs and their interaction with dislocations nucleated by indentation. Moreover, the interaction between the sessile lock and MFDs was less cared about when their distance is far sufficient as film layer thickness greater than or equal to 4 nm. The models were classified into two groups to study interaction. The group one which is Ag2/Cu and Ag3/Cu was cared about the interaction between the sessile lock and MFDs, and the group two which is Ag4/Cu and Ag5/Cu was focused on interaction between the embryonic dislocation loops and MFDs.

For the group one, the distance between the sessile lock and MFDs was close enough to create a significant attractive force which had the trend to pull each other. Due to the characteristic of a sessile dislocation, unmovable, the lock pulled and made MFDs move toward itself. Consequently, MFDs glide up to form a new defect structure as shown in Fig. 4 (a) for the case of nodded indentation. However, for the case of spaced indentation, not only the sessile lock was unable to pull two parallel MFDs gliding up, but also dislocation was glided down on the two planes of the lock by this attractive force itself, hit on these MFDs array, and then glided up on the other slip planes as shown in Fig. 4 (b).

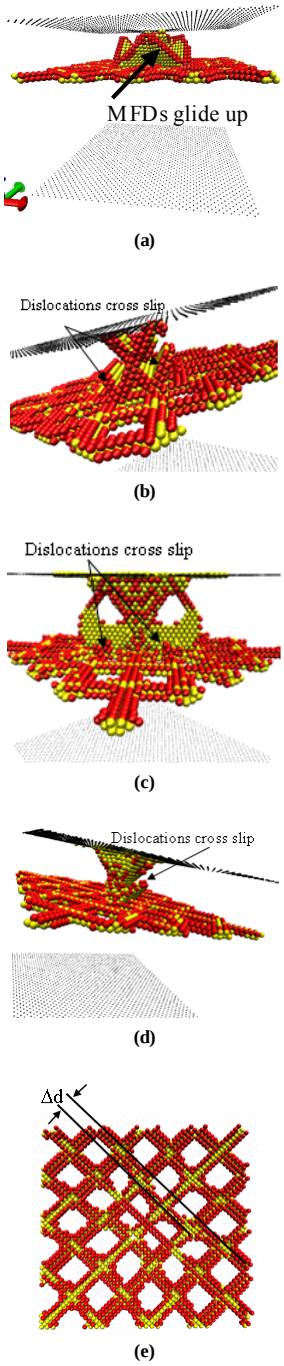


**Fig. 4 Defect structures of (a) Ag3/Cu at the depth 5.3 Å of nodded indentation, (b) Ag3/Cu at the depth 6.0 Å of spaced indentation, (c) CuAg4 at the depth 8.6 Å with cross slip of the Shockley partial dislocation at the interface, (d) Ag3/Cu at 7.8 Å under nodded indentation of the 2 nm spherical indenter tip, and (e) slip of MFDs inward the center.**

Activity of MFD in the two cases of indentation shows intersection nodes are the most unstable positions in the MFD network.

For the group two, the embryonic dislocation loop glided down on a slip plane under driving by forces from indentation and MFD attraction. As a result, the loop hit on a MFD where edge segments were firstly attracted, screw segments freely glided into a (111) adjacent slip plane. In the adjacent slip plane, the edge and screw partials exchanged their signs to create repulsive force between edge segments [38]. This repulsive force promoted the glide of partial dislocation in the new slip plane as shown in Fig. 4 (c). The changing slip plane of a dislocation, cross slip, only occurs in a bulk material as Ag under some particular conditions [38], nevertheless, It is considered that the cross slip quit easily occurred at the interface of Ag/Cu material.

The interaction between dislocations nucleated by indentation and MFDs is quite sensitive with indentation position relative to MFDs for the group one.

The interaction is affected by the distance from MFDs to the sessile lock, which is dependent on film layer thickness and size of the sessile lock. Also, the size of the sessile lock is decided by indenter tip size. The evidence for the relation is shown in Fig. 4 (d). The smaller sessile lock was nucleated in the same model of Ag3/Cu under nodded indentation with the same simulation process, but the smaller indenter tip, 2 nm spherical indenter, and resulted in dislocations cross lip at the interface.

A common phenomenon for two groups was slip of MFDs in the interface inward the center of indentation during indentation as plotted in Fig. 4 (e). This is the key factor for softening of Ag/Cu which would be discussed in detail next section.

### 3.3 Slip of MFD

Slip of MFDs causes inhomogeneous either materials, the lattice mismatch at the interface, or strain at interface due to higher stress at the upper atom layer [39]. The different strain between the upper atom and lower atom layers makes the misfit spacing various as slip of MFDs. The following analysis of misfit spacing variation verses strain of lattice constants at the interface will show the trend of MFDs slip.

The equation of misfit spacing was obtained from Eqn. (3) as follows:

$$d = \frac{1}{\sqrt{2}} \frac{a_f a_s}{|a_f - a_s|} \tag{5}$$

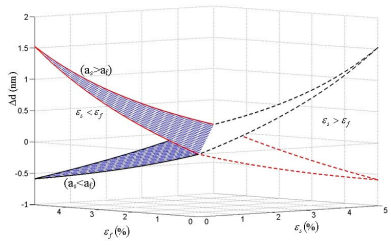


**Fig. 5 Variation of the misfit spacing.**

The deformed misfit spacing due to the strain of lattices can be evaluated with equation (6).

$$d^* = \frac{1}{\sqrt{2}} \frac{\left(a_f + \Delta a_f\right)\left(a_s + \Delta a_s\right)}{\left|\left(a_f + \Delta a_f\right) - \left(a_s + \Delta a_s\right)\right|} = \frac{1 + \varepsilon_f + \varepsilon_s}{\sqrt{2}\left|\left(1/a_f + \varepsilon_s/a_f\right) - \left(1/a_s + \varepsilon_f/a_s\right)\right|} \tag{6}$$

The difference of misfit spacing, $\Delta d = d^* - d$ , plotted in Fig. 5 shows the MFDs move inward the center as increasing of misfit spacing for the case of Ag/Cu, $a_s < a_f$, and outward the center as decreasing of misfit spacing for the contrary case such as Cu/Ag since the lattice constant of the substrate is greater than that of film, $a_s > a_f$.

Slip of dislocation, normally, is effect on the elastic energy of dislocation itself as well as energy of model. As we know, if there were no interaction between film layer and substrate layer, the indentation force would have been the same for all film layer thickness as bulk material. As shown in Fig. 2, indentation forces increase with decreasing of film layer thickness during dislocations interaction, even though the force difference occurred prior to defects nucleated by indentation. Thus, the film layer thickness and interaction between dislocation and MFDs is the main cause for difference of indentation forces. Moreover, the slip of MFDs in the interface happened during indentation as mentioned above. Therefore, the slip of MFDs may be a key factor of Ag/Cu.

The relation between the slip and indentation stress at the interface will be clear when misfit spacing is measured at the same indentation depth for all Ag/Cu models, where the stress increase with the decreasing of film layer thickness. The measurement was carried out at the indentation depth of 2.5 Å shows the initial misfit spacing without deformation of 2.175 nm was down to 1.662, 1.919, 2.163 and 2.173 nm for Ag2/Cu, Ag3/Cu, Ag4/Cu and Ag5/Cu, respectively. Slip space, subtraction of initial and deformed misfit spacing, decreases with the increasing of film layer thickness. The slip will be effect on the mechanical properties since the elastic energy per unit length of MFDs is unchanged but its length is proportional to curvature of deformed MFDs, slip space. Thus, increment of the elastic energy of MFDs is proportional to slip space. Simultaneously, the softening of the material also is inverse proportional to the increment. As a result, the slip of MFDs is a reason of softening of Ag/Cu, indentation force increase with the increasing of film layer thickness as shown in Fig. 2.

Analysis of MFD slip also shows that the indentation force of Ag/Cu will be closer to that of bulk Ag when slip is very small, it also means that the film layer is thicker. The relation between yield force and film layer thickness using the data in table 1 was plotted in Fig. 6. In which critical thickness is where the softening rule is not held, yield force of thicker films is the same as that of bulk Ag. The spline extrapolation based on that data shows the critical film thickness of Ag is equal to 6.632 nm. The same process was carried out for Cu (001)/Ag (001) models, and the critical Cu film layer thickness was calculated to be equal to 5.402 nm which is well agreement with the calculations of the Cu critical grain size from 3.3 to 6.6 nm [40-43].

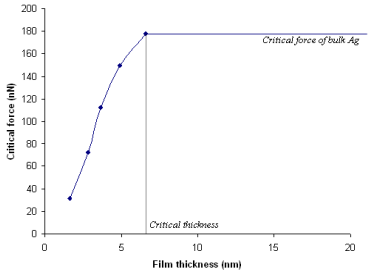


**Fig. 6 Yield force-film thickness curve.**

## 4. Conclusions

Atomistic simulation of nanoindentation on Ag (001)/Cu (001) using EAM was carried out to investigate MFD slip. The simulation shows the indentation position relative to MFD is strong effect on the actions of MFDs, glide up or cross slip, for Ag2/Cu and Ag3/Cu but less effect on thicker film layer, Ag4/Cu and Ag5/Cu. Elastic energy variation during MFDs slip was revealed a key factor for the softening of Ag/Cu, indentation force decreases with decreasing of film layer thickness. The critical film layer thickness of

Ag and Cu was calculated based on simulation results of film/substrate and bulk material of the film using spline extrapolation technique. The calculation results for Ag and Cu are good agreement with previously published results.

## Acknowledgements

This study was supported by the ministry of knowledge and economy under the grant number of 10028421-2010-22.

## References

1) Phong, "Investigation of antibacterial activity of cotton fabric incorporating nano silver colloid," *J. Physics: Conference Series*, Vol. 187, 2009, p. 012072.
2) H. Wang, J. Wang, J. Hong, Q. Wei, W. Gao and Z. Zhu, "Preparation and characterization of Ag nanocomposite textile," *J. Coating Technology Research*, Vol. 4, 2007, pp. 101-106.
3) P. S. Phani, D. S. Rao, S. V. Joshi and G. Sundararajan, "Effect of process parameters and heat treatments on properties of cold sprayed Cu coatings," *J. Thermal Spray Technology*, Vol. 16, 2007, pp. 425-434.
4) S. Q. Wang, H. Zhao, Y. Wang, C. M. Li, Z. H. Chen and V. Paulose, "Ag-coated near field optical scanning microscope probes fabricated by Ag mirror reaction," *Applied Physics B*, Vol. 92, 2008, pp. 49-52.
5) P. Wróbel, J. Pniewki, T. J. Antosiewicz and T. Szoplik, "Focusing radially polarized light by concentrically corrugated Ag film without a hole," *Physical Review letters*, Vol. 102, 2009, p. 183902.
6) G. Bartal, G. Lerosey and X. Zhang, "Subwavelength dynamic focusing in plasmonic nanostructures using time reversal," *Physical Review B*, Vol. 79, 2009, p. 201103.
7) S. Nakahara and E.C. Felder, "Generation of grown-in dislocations at Ni-Cu misfit boundaries during three-dimensional nucleation and growth," *Thin Solid Films*, Vol. 91, 1982, pp. 111-122.
8) A. Misra, J. P. Hirth and H. Kung, "Single-dislocation-based strengthening mechanisms in nanoscale metallic multilayers," *Philosophical Magazine A*, Vol. 82, 2002, pp. 2935-2951.
9) "Microstructures and strength of nanoscale Cu-Ag multilayers," *Scripta Materialia*, Vol. 46, 2002, pp. 593-598.
10) "The deformation and ageing of mild steel: III discussion of results," *Proceeding of Physical Society B*, Vol. 64, 1951, pp. 747-753.
11) "The cleavage strength of polycrystals," *J. Iron Steel Institute*, Vol. 174, 1953, pp. 25-28.
12) Hull and D. J. Bacon, "Introduction to Dislocations," 4th ed., Butterworth-Heinemann, Oxford 2001, chapter 5.
13) "Cracking and adhesion at small scales: atomistic and continuum studies of flaw tolerant nanostructures," *Modelling and Simulation in Materials Science and Engineering*, Vol. 14, 2006, pp. 799-816.
14) S. M. Han, M. A. Phillips and W. D. Nix, "Study of strain softening behavior of Al-Al3Sc multilayers using microcompression testing," *Acta Materialia*, Vol. 57, 2009, pp. 4473-4490.
15) H. V. Swygenhoven, M. Spaczer, A. Caro and D. Farkas, "Competing plastic deformation mechanisms in nanophase metals," *Physical Review B*, Vol. 60, 1999, p. 22.
16) H. V. Swygenhoven, P. M. Derlet and A. Hasnaoui, "Atomic mechanism for dislocation emission from nanosized grain boundaries," *Physical Review B*, Vol. 66, 2002, p. 024101.
17) A. Jerusalem and R. Radovitzky R, "A continuum model of nanocrystalline metals under shock loading," *Modelling and Simulation in Materials Science and Engineering*, Vol. 17, 2009, p. 025001.
18) D. Saraev D and R. E. Miller, "Atomic-scale simulation of nanoindentation-induced plasticity in copper crystals with nanometer-sized nickel coatings," *Acta Materialia*, Vol. 54, 2006, pp. 33-45.
19) W. C. Oliver and G. M. Pharr, "Measurement of hardness and elastic modulus by instrumented indentation: Advances in understanding and refinements to methodology," *J. Materials Research*, Vol. 19, 2004, pp. 3-20.
20) R. Smith R, D. Christopher and S. D. Kenny, "Defect generation and pileup of atoms during nanoindentation of Fe single crystals," *Physical Review B*, Vol. 67, 2003, p. 245405.
21) M. S. Daw and M. I. Baskes, "Embedded-atom method: Derivation and application to impurities, surfaces, and other defects in metals," *Physical Review B*, Vol. 29, 1984, pp. 6443-6453.
22) S. M. Foiles, M. I. Baskes and M. S. Daw, "Embedded-atom-method functions for the fcc metals Cu, Ag, Au, Ni, Pd, Pt, and their alloys," *Physical Review B*, Vol. 33, 1986, pp. 7983-7991.
23) "Atomistic modeling of the γ and γ′-phases of the Ni-Al system," Acta Materialia, Vol. 52, 2004. pp. 1451-1467.
24) F. Heringhaus, H. J. Schneider and G. Gottstein, "Analytical

modeling of the electrical conductivity of metal matrix composites: application to Ag-Cu and Cu-Nb," *Materials Science and Engineering A*, Vol. 347, 2003, pp. 9-20.
25) D. W. Yao and L. Meng, "Effects of solute, temperature and strain on the electrical resistivity of Cu-Ag filamentary composites," *Physica B*, Vol. 403, 2008, pp. 3384-3388.
26) Y. T. Ning, X. H. Zhang and Y. J. Wu, "Electrical conductivity of Cu-Ag in situ filamentary composites," *The Transactions of Nonferrous Metals Society of China*, Vol. 17, 2007, pp. 378-383.
27) N. W. Ashcroft and N. D. Mermin, *Solid State Physics*, Harcourt College Publishers, New York, 1976.
28) H. N. G. Wadley, X. W. Zhou, R. A. Johnson and M. Nuerock, "Mechanisms, models and methods of vapour deposition," *Progress in Materials Science*, Vol. 46, 2001, p. 329.
29) R. A. Johnson, "Alloy models with the embedded atom method," *Physical Review B*, Vol. 39, 1989, p. 12554.
30) C. L. Kelchner, S. J. Plimpton and J. C, Hamilton, "Dislocation nucleation and defect structure during surface indentation," *Physical Review B*, Vol. 58, 1998, p. 11085.
31) E. T. Lilleodden, J. A. Zimmerman, S. M. Foiles and W. D. Nix, "Atomistic simulations of elastic deformation and dislocation nucleation during nanoindentation," *J. Mechanics and Physics of Solids*, Vol. 51, 2003, pp. 901-920.
32) S. Nose, "A unified formulation of the constant temperature molecular dynamics methods," *J. Chemical Physics*, Vol. 81, 1984, p. 511.
33) W. G. Hoover, "Canonical dynamics: Equilibrium phase-space distributions," *Physical Review A*, Vol. 31, 1985, p. 1695.
34) S. J. Plimpton and B. A. Hendrickson, "In: J. Broughton, P. Bristowe, J. Newsam, (editors), Materials theory and modelling," *MRS Proceedings*, Vol. 291, 1993, p. 37 Pittsburg(PA).
35) 트란딘 룽, 김엄기, 전성식, "분자동력학 해석을 이용한 인덴테이션시 실리콘 내부의 결함구조에 관한 연구," 한국복합재료학회 논문집, Vol. 22, 2009, pp. 9-17.
36) K. J. Van Vliet, J. Li, T. Zhu, S. Yip and S. Suresh, "Quantifying the early stages of plasticity through nanoscale experiments and simulations," *Physical Review B*, Vol. 67, 2003, p. 104105.
37) J. Lian, J. Wang, Y. Y. Kim and J. Greer, "Sample boundary affect in nanoindentation of nano and microscale surface structures," *J. the Mechanics and Physics of Solids*, Vol. 57, 2009, pp. 812-827.
38) G. Lu, V. V. Bulatov and N. Kioussis, "Dislocation constriction and cross-slip: An ab initio study," *Physical Review B*, Vol. 66, 2002, p. 144103.
39) A. C. Fisher-Cripps, *Introduction to contact mechanics*, 2nd ed., Springer, New York, 2007.
40) J. Schiotz and K. W. Jackobsen, "A Maximum in the Strength of Nanocrystalline Copper," *Science*, Vol. 301, 2003, pp. 1357-1359.
41) S. Yip, "The Strongest Size," *Nature*, Vol. 391 1998, pp. 532-533.
42) K. W. Jackobsen and J. Schiotz, "Computational materials science: Nanoscale plasticity," *Natural Materials*, Vol. 1, 2002, pp. 15-16.
43) P. G. Sanders, J. A. Eastman and J. R. Weertman, "Elastic and tensile behavior of nanocrystalline copper and palladium," *Acta Materialia*, Vol. 45, 1997, pp. 4019-4025.